Selenium substitution effect on crystal structure of stibnite (Sb_2S_3)

Atsushi Kyono[1,*], Akinobu Hayakawa,[2] and Mayumi Horiki[2]

[1]Division of Earth Evolution Sciences, Graduate School of Life and Environmental Sciences,

University of Tsukuba, 1-1-1 Tennodai, Tsukuba, Ibaraki 305-8572, Japan

[2]High Performance Plastics Company, Sekisui Chemical Co., Ltd.

2-1 Hyakuyama, Shimamoto Chou, Mishima Gun, Osaka 618-0021, Japan

Correspondence author: A. Kyono

Address: Division of Earth Evolution Sciences, Graduate School of Life and Environmental Sciences,

University of Tsukuba, 1-1-1 Tennodai, Tsukuba, Ibaraki 305-8572, Japan

Correspondence e-mail: kyono@geol.tsukuba.ac.jp

Phone: +81-29-853-7176, Fax: +81-29-853-7887

ABSTRACT

Composition dependence of the crystal structure between stibnite and antimonselite is investigated by using the single-crystal x-ray diffraction and the *ab-initio* calculation methods to clarify the Se substitution effect on the crystal structure, especially focusing on the stereochemical behavior of Sb $5s^2$ lone pair electrons. The single-crystal x-ray diffraction measurements indicate no phase change throughout the solid solution range. The lattice parameters of *a*, *b*, *c* and unit cell volume are linearly increased as Se content increases. The lattice parameter variations normalized show an anisotropic expansion that the largest expansion is observed along the ***a***-axis, followed by the ***c*** and ***b***-axes. The large Se atom exhibits a strong site preference for the X(1) and X(3) sites, while the small S atom prefers to occupy the X(2) site. The intra-ribbon Sb(1)-X and Sb(2)-X distances (X = S, Se) are continuously increased with the Se content. The three Sb(1)-X bond distances in the trigonal pyramids are changed within the similar range between 2.52 and 2.68 Å, while the five Sb(2)-X distances in the tetragonal pyramids vary from 2.45 to 2.59 Å, from 2.68 to 2.80 Å, and from 2.86 to 3.00 Å, respectively. With increasing Se content in the solid solution, the inter-ribbon distances where the Sb $5s^2$ LPEs are located monotonously increase as well. However, the variations between the ribbons are considerably smaller than those of intra-ribbon distances. The polyhedral volumes of the $Sb(1)X_7$ and $Sb(2)X_7$ in which the Sb $5s^2$ LPEs are accommodated constantly increase from 35.9 to 40.0 $Å^3$ and from 34.1 to 38.8 $Å^3$, respectively, and these eccentricity parameters decrease from 0.66 to 0.62 and

from 0.57 to 0.55. As a result of *ab-initio* calculation, the Sb 5s orbitals on the Sb(1) atoms remain almost unchanged throughout the solid solution. On the other hand, the those on the Sb(2) atoms become smaller with the incorporation of Se. The result gives a more reasonable interpretation that the stereochemistry of Sb $5s^2$ LPEs and the stereochemisry of the coordination polyhedra around the Sb atoms are affected by the Se substitution in the structure.

Key words: stibnite, antimonselite, stereochemical activity, single-crystal x-ray diffraction, *ab-initio* calculation

INTRODUCTION

Stibnite (Sb_2S_3) is an antimony sulfide mineral which occurs most commonly in hydrothermal vein and replacement deposits of low-temperature origin (e.g., Wood et al. 1987; Krupp 1988; Gaines et al. 1997). It is found in association with minerals such as realgar, orpiment, cinnabar, galena, pyrite, arsenopyrite, calcite, and quartz (Anthony et al. 1990). The crystal structure consists of parallel $(Sb_4S_6)_n$ ribbon-like chains held together with the weaker intermolecular forces (Hofmann 1933; Scavnicar 1960; Bayliss and Nowacki 1972). In the crystal structure, Sb atoms in a trivalent state are distributed over two different crystallographic sites. The two crystallographically independent Sb atoms exhibit a characteristic one-sided coordination because of the stereochemical activity of inert $5s^2$ lone-pair electrons (LEPs) of the Sb atoms (Kyono et al. 2002; Kyono and Kimata 2004). One shows a trigonal SbS_3 pyramid with the Sb atom at the vertex, and another forms an SbS_5 square pyramid with the Sb atom at the centre. An isomorphic mineral of the stibnite, antimonselite Sb_2Se_3, has also been known (Chen et al. 1993; Jambor and Grew 1994; Min et al. 1998). Liu et al. (2008) indicated that there is a continuous solid solution between stibnite and antimonselite. The Se/S ratios can be used as a typical geochemical indicator of deposition in a volcanic environment because the Se/S ratio is useful for determining not only the sources of S but also geothermometry and the redox gradients (Anderson 1969; Huston et al. 1995). A variety of stereochemical activities induced by the LPEs drastically affect configuration of stibnite because the Sb $5s^2$ LPEs are interposed between the

ribbon-like chains running along the ***b***-axis (Kyono and Kimata 2004). Thus, the stereochemically active LPEs play an important role in determining the structural stability. It has been known that a phase transition in a stibiocolumbite-bismutocolumbite solid solution is caused by varying degree of stereochemical activity (Kazantsev et al. 2002). However, little is known about the detailed influence of substitution of S with Se on the stereochemical activities of Sb $5s^2$ LPEs and crystal structure. Recently, the Sb_2S_3 and Sb_2Se_3 have been enthusiastically studied as one of the most promising materials for low cost and high efficiency thin film solar cells (Fernández and Merino 2000; Rajpure and Bhosale 2000, 2002; Zheng et al. 2002; Messina et al. 2009; Patrick and Giustino 2011; Choi et al 2014). The thin films with the composition of $Sb_2S_xSe_{3-x}$ have an optical band gap of 1.3–1.7 eV along the thickness (Messina et al. 2007), which would be an attractive feature for solar cells. In order to comprehend the electronic structure of the materials, it is necessary to fully understand the behavior of crystal structure, stereochemical activity of Sb $5s^2$ LEPs, and distribution of the anions within the range from Sb_2S_3 to Sb_2Se_3.

Here we present the results of the single-crystal x-ray diffraction study of the compositions between stibnite and antimonselite and the *ab-initio* theoretical study of the electronic structures. The experimental and theoretical results obtained in the present study clearly show the Se substitution effect on the crystal structure, especially focusing on the stereochemical behavior of Sb $5s^2$ LPEs in the solid solution.

EXPERIMENTAL METHODS

Commercially available Sb (Wako Pure Chemical, purity > 99.5%), S (Wako Pure Chemical, purity > 98.0%), and Se metal (Wako Pure Chemical, purity > 99.0%) were used as starting materials. Compositions of the starting mixtures were as follows: Sb:S:Se ratio of (1) 2 : 3 : 0, (2) 2 : 2.25 : 0.75, (3) 2 : 1.5 : 1.5, (4) 2 : 0.75 : 2.25, and (5) 2 : 0 : 3. The mixed powders were sealed under vacuum in a quartz vessel. It was subsequently placed into a furnace and heated at 500 °C for 96 h. Finally, elongated prismatic single crystals with a length of 100-300 μm were obtained.

For single-crystal x-ray diffraction measurements, suitable single crystals were fixed on a 0.1 mm diameter glass fiber, and then mounted on a RAXIS-RAPID imaging plate diffractometer (Rigaku Corp.) operating with Mo*K*α radiation (λ = 0.71069 Å) monochromatized using a flat graphite crystal. A data set of 44 images was collected using an ω-oscillation method with 5.0° oscillation step between 130 and 190° (χ = 45°, φ = 0°) and between 0 and 160° (χ = 45°, φ = 180°). The exposure rate was of 180 s per degree of the oscillation. Intensities were corrected for Lorentz and polarization effects. An absorption correction was applied from the symmetry-equivalent reflections using the ABSCOR program (Higashi 1995). The structure was solved using direct methods with the SIR97 program package (Altomare et al. 1999). Only reflections with $I_o > 4\sigma(I_o)$ were used for structure refinements performed using full-matrix least squares on F^2 with the CRYSTALS program (Carruthers et al. 1999).

After the all x-ray diffraction measurements, each single crystal was removed and mounted in epoxy. Then it was polished using a 1 μm diamond suspension for the electron microprobe analysis. Quantitative chemical analysis was performed with the JXA-8530F electron probe micro-analyzer (JEOL Ltd.) equipped with a wavelength-dispersive x-ray spectrometer. The samples were probed with an acceleration voltage of 15 kV, an irradiation current of 10 nA, and a beam diameter of 1 μm. The chemical composition of each crystal was determined from the averages of several points analyzed. Raw data were corrected using a conventional ZAF program. Synthetic Sb_2S_3 (Sb*L*α and S*K*α) and synthetic Sb_2Se_3 (Se*L*α) were used as standards. Empirical formulae were normalized on the basis of five atoms per formula unit. Site occupancies were refined within the constraint that three X sites (X = S, Se) are occupied fully by the S and Se atoms. Based on the assumption that the S and Se atoms are disordered at three X sites, the ratio between S and Se was refined under the constraint that total S/Se ratio is equal to the chemical composition determined with the electron microprobe analyses. Data collection and refinement details are reported in Table 1. The final atomic positions and their chemical compositions are presented in Table 2. All bond lengths and bond angles are given in Table 3.

Ab-initio calculations of the electronic structure were performed at DFT/B3LYP/3-21+G basis set using the quantum chemical calculation software package Gaussian-09 (Frisch et al. 2009). Initial structure models were built based on the atomic coordinates experimentally determined by the x-ray

diffraction measurement in the present study. The dimension of the simulation region includes four characteristic ribbon-like chains. To terminate an infinite crystal structure, hydrogen atoms were added as a positive charge on the S and Se atoms at the terminal positions. The orbital surfaces were rendered with the GaussView molecular visualization package (Dennington et al. 2009). The orbitals were drawn at an interface value of 0.02.

RESULTS AND DISCUSSION

The single-crystal x-ray diffraction measurements indicate no phase change occurs throughout the solid solution range. The $Sb_2S_{3-x}Se_x$ ($0 \leq x \leq 3$) can form a complete solid solution between Sb_2S_3 and Sb_2Se_3. The variations in lattice parameters are summarized in Figure 1. Data were fitted by a least-squares regression to the second degree polynomial curve. With increasing Se content, the lattice parameters of ***a***, ***b***, and ***c*** are linearly increased from 11.33 to 11.80 Å, from 3.84 to 3.99 Å, and from 11.25 to 11.65 Å, respectively. As a result of expansion of the lattice parameters, the unit cell volume undergoes a monotonous increase from 489 to 548 $Å^3$ as a function of the Se content (Table 1). The lattice parameter variations normalized to the minimum values show an anisotropic expansion of the lattice parameters against the Se content (Fig. 1d). The largest expansion is observed along the ***a***-axis, followed by the ***c*** and ***b***-axes (Fig. 1d). The anisotropic behavior with the Se content is exactly identical to those induced by compression (Lundegaard et al. 2003). At a temperature range from 128 to 298 K,

the largest thermal expansion occurs along the ***c***-axis, followed by the ***a***, and ***b***-axes (Kyono et al. 2002). The anisotropic behavior of the orthorhombic lattice is reflected by the structural characteristic feature. As can be seen in Figure 2a, there are a lying trigonal pyramid at the Sb(1) position and a standing tetragonal pyramid at Sb(2) position along the ***b***-axis. The ***b***-axis direction is most rigid due to the strong bonded ribbon structure, which reflects the smallest expansion behavior of ***b***-axis. On the other hand, the space between the ribbons running parallel to ***b***-axis accommodates the Sb $5s^2$ LPEs. Because the electron density is concentrated within the ribbons, Sb-X (X = S, Se) bonds between ribbons become much weaker than those within the ribbons. That is, the ***a***- and ***c***-axes directions are most variable due to the weak interactions between the ribbons. The site-occupancy parameters of Se over the three X sites are plotted in Figure 3. The large Se atom exhibits a strong site preference for the X(1) and X(3) sites, while the small S atom prefers to occupy the X(2) site. This is because the atomic positions of X(1) and X(3) can maintain the longer distance from Sb atoms than the X(2) position.

The variations of the intra-ribbon Sb-X distances are shown in Figures 4 and 5. The intra-ribbon Sb(1)-X and Sb(2)-X distances are continuously increased with the Se content. The three Sb(1)-X bond distances in the trigonal pyramids are changed within the similar range of 2.52 to 2.68 Å, while the five Sb(2)-X distances in the tetragonal pyramids vary from 2.45 to 2.59 Å, from 2.68 to 2.80 Å, and from 2.86 to 3.00 Å, respectively (Figs 4, 5). Although the ranges are considerably different from

one another, the variations of the Sb(1)-X distances exhibit similar elongation behavior to the Sb(2)-X. That is, since the short bondings possess a strong electrostatic interaction between Sb and S/Se atoms, the short bond distances are more changeable than the long bond distances by the substitution of S with Se (Figs 4d, 5d). The Sb(1)-X(2) distance located within the ribbon-like structure changes from 3.12 to 3.22 Å with the Se content (Fig 4c). The slight variation of the Sb(1)-X(2) distance is due to the rather long distance over 3.10 Å (Fig. 4d).

The variations of the inter-ribbon Sb-X (X = S, Se) distances are given in Figure 6. As the Se content increases in the solid solution, the inter-ribbon distances where the Sb $5s^2$ LPEs are located monotonously increase as well. With the substitution of S with Se, the Sb(1)-X(1) and Sb(2)-X(3) distances are extended from 3.64 to 3.74 Å, and from 3.38 to 3.48 Å, respectively (Figs 6b, 6c). However, the variations between the ribbons are considerably smaller than those of intra-ribbon distances. The electron density of Sb $5s^2$ lone pair electrons is fairly smaller than those of antimony atoms. Only the Sb $5s^2$ lone pair electrons can't be observed within the electron density distribution of antimony atoms. In order to assess the Se substitution effect on the stereochemical activity of Sb $5s^2$ LEPs, therefore, the polyhedral volumes and eccentric parameters of two sevenfold coordinations including the LPEs (Fig. 2b) are calculated by the IVTON program (Balić-Žunić and Vickovic 1996). The polyhedral volumes of the $Sb(1)X_7$ and $Sb(2)X_7$ constantly increase from 35.9 to 40.0 $Å^3$ and from 34.1 to 38.8 $Å^3$, respectively (Fig. 7a, 7b). The eccentric parameter is defined as the deviation of

central atom position from the ideal metric centre of the coordination. That is, the larger the eccentricity suggests the larger stereochemical activity. As it can be seen from Figures 7c and 7d, the stereochemical deformation seems to decrease from 0.66 to 0.62 at $Sb(1)X_7$ and from 0.57 to 0.55 at $Sb(2)X_7$ with increase of the Se concentration. The stereochemical activity in the $Sb(1)X_7$ polyhedron is larger than that in the $Sb(2)X_7$ polyhedron. In the solid solution between Sb_2S_3 and Bi_2S_3 (Kyono and Kimata, 2005), however, the eccentric parameter drastically decreases with the Bi concentration from 0.66 to 0.42 at the $M(1)X_7$ coordination (M = Sb, Bi) and from 0.57 to 0.48 at the $M(2)X_7$ coordination. A more reasonable interpretation is therefore presented that the stereochemistry of Sb $5s^2$ LPEs is only slightly affected by the Se substitution in the crystal structure.

During the past decade, several first principle studies have been carried out on the structural and electronic properties of Sb_2S_3 and Sb_2Se_3 (Caracas and Gonze 2005; Patrick and Giustino, 2011; Koc et al. 2012; Filip et al. 2013). The valence electron density, the electron band structure, and the corresponding electronic density-of-states were examined using the density functional theory (Koc et al. 2012). The authors determined the valence-band energy levels in the structures. As the results, the highest occupied valence bands are essentially dominated by S 3p, Se 4p, and Sb 5p states. The Sb 5s states dominate the second energy group with small electronic density-of-states of the S 3s, 3p and the Se 4s, 4p. Figure 8 shows the molecular orbitals associated with the stereochemical activity of Sb $5s^2$ LPEs. In the energy level of Sb_2S_3 (Fig. 8a), the Sb 5s orbitals occupy the overlying spaces of the Sb

atoms, resulting in a formation of the characteristic one-sided coordination of the Sb atom. A few Sb atoms without the characteristic LPEs are also observed. In the study, the dimension of the simulation region includes four ribbon-like chains. As it can be seen in the Fig. 8a, the electronic orbitals are almost equally spread over a whole ribbon. On the other hand, the electronic orbitals in the structure introducing a small amount of Se atoms are shown in Fig.8b. Since the Se atom exhibits a strong site preference for the X(1) (Fig. 3), the Se atoms are distributed on the X(1) sites in the structure. The most noteworthy finding is that the electronic orbitals are highly delocalized with substitution of Se for S atoms (Fig. 8b). Compared with the pure Sb_2S_3, most electronic orbitals are reduced in the two ribbons lying on the upper and lower ribbons. The Sb 5s orbitals on the Sb(1) atoms remain almost unchanged, whereas those on the Sb(2) atoms in the upper and lower side become smaller with the incorporation of Se into the structure (Fig. 8b). The electronic orbitals in the Sb_2Se_3 are displayed in Fig. 8c. It exhibits an essentially similar feature to that of the $Sb_2(S_2Se)_3$ (Fig. 8b). The highly delocalized electronic orbitals in each ribbon are observed as well. In Sb_2Se_3, however, the electronic orbitals distributed in the two ribbons lying on the upper and lower ribbons are much reduced compared with those of the $Sb_2(S_2Se)_3$. Accordingly, the electronic orbitals in stibnite are significantly influenced by the Se substitution for S atoms. The results of the *ab-initio* theoretical study are approximately consistent with those of the x-ray diffraction measurement given in Figures 7c and 7d. In the structure, stereochemical arrangement is caused by the repulsive electrostatic interaction

between the LPEs of the stereochemically active central Sb atom and coordinated ligands. That is, the stereochemistry in the structure would be affected not only by the Sb 5s orbitals but the highest occupied valence bands dominated by S 3p, Se 4p, and Sb 5p. The electronic orbitals of the S 3p, Se 4p, and Sb 5p are not considered in the study, but the *ab-initio* calculation reveals that the electronic orbitals, especially Sb 5s orbitals, are drastically affected by the incorporation of Se into the stibnite structure. As mentioned before, the change in stereochemical configuration induced by the Se substitution is smaller than that caused by the Bi substitution (Kyono and Kimata, 2005), although variations of the *a* and *c* lattice parameters between Sb_2S_3 and Sb_2Se_3 are significantly larger than those between Sb_2S_3 and Bi_2S_3. In conclusion, the stereochemical feature of Sb $5s^2$ LEPs and the stereochemisry of the coordination polyhedra around the Sb atoms can be reduced with the Se substitution for S in stibnite.

ACKNOWLEDGMENTS

We thank E. Makovicky and an anonymous reviewer for their constructive comments and T. Tsuchiya for editorial handling. We are grateful to N. Chino for kindly providing technical help with the EPMA analyses. The work was partially supported by a Grant-in-Aid for Young Scientists (B) from the Japan Society for the Promotion of Science (project no. 24740352).

REFERENCES

Altomare A, Burla MC, Camalli M, Cascarano GL, Giacovazzo C, Guagliardi A, Moliterni AGG, Polidori G, Spagna R (1999) SIR97: a new tool for crystal structure determination and refinement. Journal of Applied Crystallography 32: 115–119

Anderson CA (1969) Massive sulfide deposits and volcanism. Economic Geology 64: 129–146

Anthony JW, Bideaux RA, Bladh KW, Nichols MC (1990) Handbook of mineralogy Vol. I. Elements, Sulfides, Sulfosalts. Mineral Data Publishing, Tucson, Arizona, p498

Balić-Žunić T, Vickovic I (1996) IVTON—program for the calculation of geometrical aspects of crystal structures and some crystal chemical applications. Journal of Applied Crystallography 29: 305–306

Bayliss P, Nowacki W (1972) Refinement of the crystal structure of stibnite, Sb_2S_3. Zeitschrift für Kristallographie 135: 308–315

Caracas R, Gonze X (2005) First-principles study of the electronic properties of A_2B_3 minerals, with A=Bi,Sb and B=S,Se. Physics and Chemistry of Minerals, 32: 295–300

Carruthers JR, Rollett JS, Betteridge PW, Kinna D, Pearce L, Larsen A, Gabe E (1999) CRYSTALS No. 11. Chemical Crystallography Laboratory, Oxford, U.K.

Chen L, Zhang Q, Li D, Wang G (1993) Antimonelite: A new mineral. Acta Mineralogica Sinica 13: 7–11 (in Chinese with English abs.)

Choi YC, Mandal TN, Yang WS, Lee YH, Im SH, Noh JH, Seok SI (2014) Sb_2Se_3-sensitized inorganic-organic heterojunction solar cells fabricated using a single-source precursor. Angewandte Chemie International Edition 53: 1329–1333

Dennington R, Keith T, Millam J (2009) GaussView, Version 5, Semichem Inc., Shawnee Mission KS

Fernández AM, Merino MG (2000) Preparation and characterization of Sb_2Se_3 thin films prepared by electrodeposition for photovoltaic applications. Thin Solid Films 366: 202–206

Filip MR, Patrick CE, Giustino F (2013) GW quasiparticle band structures of stibnite, antimonselite, bismuthinite, and guanajuatite. Physical Review B, 87: 205125

Frisch MJ, Trucks GW, Schlegel HB, Scuseria GE, Robb MA, Cheeseman JR, Scalmani G, Barone V, Mennucci B, Petersson GA, Nakatsuji H, Caricato M, Li X, Hratchian HP, Izmaylov AF, Bloino J, Zheng G, Sonnenberg JL, Hada M, Ehara M, Toyota K, Fukuda R, Hasegawa J, Ishida M, Nakajima T, Honda Y, Kitao O, Nakai H, Vreven T, Montgomery Jr.JA,

Peralta JE, Ogliaro F, Bearpark M, Heyd JJ, Brothers E, Kudin KN, Staroverov VN, Kobayashi R, Normand J, Raghavachari K, Rendell A, Burant JC, Iyengar SS, Tomasi J, Cossi M, Rega N, Millam JM, Klene M, Knox JE, Cross JB, Bakken V, Adamo C, Jaramillo J, Gomperts R, Stratmann RE, Yazyev O, Austin AJ, Cammi R, Pomelli C, Ochterski JW, Martin RL, Morokuma K, Zakrzewski VG, Voth GA, Salvador P, Dannenberg JJ, Dapprich S, Daniels AD, Farkas Ö, Foresman JB, Ortiz JV, Cioslowski J, Fox DJ, (2009) Gaussian 09, Revision A.1, Gaussian, Inc., Wallingford CT

Gaines RV, Skinner HCW, Foord EE, Mason B, Rosenzweig A (1997) Dana's new mineralogy: the system of mineralogy of James Dwight Dana and Edward Salisbury Dana, 8th ed. John Wiley, New York, p106

Higashi T (1995) Abscor–Empirical absorption correction based on Fourier series approximation. Rigaku Corp. Tokyo

Hofmann W (1933) Die Struktur der Minerale der Antimonitgruppe. Zeitschrift für Kristallographie 86: 225–245

Huston DL, Sie SH, Suter GF, Cooke DR, Both RA (1995) Trace elements in sulfide minerals from eastern Australian volcanic-hosted massive sulfide deposits: part I. Protein microprobe analyses of pyrite, chalcopyrite and sphalerite, and part II. Selenium levels in pyrite: comparison with δ34S values and implications for the source of sulfur in volcanogenic

hydrothermal systems. Economic Geology 90: 1167–1196

Jambor JL, Grew ES (1994) New mineral names. American Mineralogist 79: 387–391

Kazantsev SS, Pushcharovsky DY, Maximov BA, Molchanov NV, Werner S, Schneider J, Sapozhnikov AN (2002) Phase transitions in solid solution series bismutocolumbite-stibiocolumbite (Bi-Sb)($Nb_{0.79}Ta_{0.21}$)O_4. Zeitschrift für Kristallographie 217: 542–549

Koc H, Mamedov AM, Deligoz E, Ozisik H (2012) First principles prediction of the elastic, electronic, and optical properties of Sb_2S_3 and Sb_2Se_3 compounds. Solid State Sciences, 14: 1211–1220

Krupp RE (1988) Solubility of stibnite in hydrogen sulfide solutions, speciation, and equilibrium constants, from 25 to 350°C. Geochimica et Cosmochimica Acta 52: 3005–3015

Kyono A, Kimata M, Matsuhisa M, Miyashita Y, Okamoto K (2002) Low-temperature crystal structures of stibnite implying orbital overlap of Sb $5s^2$ inert pair electrons. Physics and Chemistry of Minerals 29: 254–260

Kyono A, Kimata M (2004) Structural variations induced by difference of the inert pair effect in the stibnite-bismuthinite solid solution series $(Sb,Bi)_2S_3$. American Mineralogist 89: 932–940

Liu JJ, Liu JM, Li JL, Xie H, Wang JP, Deng J, Feng C, Qi F, Zhang N (2008) Experimental synthesis of the stibnite-antimonselite solid solution series. International Geology Review 50:

168–176

Lundegaard LF, Miletich R, Balic-Zunic T, Makovicky E (2002) Equation of state and crystal structure of Sb_2S_3 between 0 and 10 GPa. Physics and Chemistry of Minerals, 30: 463–468

Messina S, Nair MTS, Nair PK (2007) Antimony sulfide thin films in chemically deposited thin film photovoltaic cells. Thin Solid Films 515: 5777–5782

---------- (2009) Antimony selenide absorber thin films in all-chemically deposited solar cells. Journal of the Electrochemical Society 156: H327–H332

Min MZ, Zhai JP, Wang XY, Shen BP, Wen GD, Fan, T (1998) Refinement of the crystal structure for a new mineral – antimonselite. Chinese Science Bulletin 43: 413–416

Patrick CE, Giustino F (2011) Structural and electronic properties of semiconductor-sensitized solar-cell interfaces. Advanced Functional Materials 21: 4663–4667

Rajpure KY, Bhosale CH (2000) Sb_2S_3 semiconductor-septum rechargeable storage cell. Materials Chemistry and Physics 64: 70–74

---------- (2002) Preparation and characterization of spray deposited photoactive Sb_2S_3 and Sb_2Se_3 thin films using aqueous and non-aqueous media. Materials Chemistry and Physics 73: 6–12

Scavnicar S (1960) The crystal structure of stibnite. A redetermination of atomic positions. Zeitschrift

für Kristallographie 14: 86–97

Wood SA, Crerar DA, Borcsik MP (1987) Solubility of the assemblage pyrite-pyrrhotite-magnetite-sphalerite-galena-gold-stibnite-bismuthinite-argentite-molybdenite in H_2O-NaCl-CO_2 solutions from 200°C to 350°C. Economic Geology 82: 1864-1887

Zheng XW, Xie Y, Zhu LY, Jiang XC, Jia YB, Song WH, Sun YP (2002) Growth of Sb_2E_3 (E = S, Se) polygonal tubular crystals via a novel solvent-relief-self-seeding process. Inorganic Chemistry 41: 455–461

Captions for Figures and Tables

Figure 1 The compositional dependence lattice parameters of (a) *a*, (b) *b*, and (c) *c*. (d) The variations of normalized lattice parameters divided by minimum values for each lattice parameter. Solid circles, open diamonds, and solid triangles stand for the a/a_0, b/b_0, and c/c_0, respectively. Data were fitted by a least-squares regression to the second degree polynomial curve. The error bars are smaller than the data points.

Figure 2 A ball-and-stick view of the crystal structure of Sb_2X_3 (X=S, Se) viewed in the direction of *b*-axis.

Figure 3 Site occupancy parameters for Se on the three X sites in the $Sb_2S_{3-x}Se_x$ solid solution. Solid circles, solid triangles, and open diamonds indicate the X(1), X(2), and X(3) site, respectively.

Figure 4 Variations of Sb-X (X= S, Se) bond lengths around the Sb1 site. The error bars are smaller than the data points.

Figure 5 Variations of Sb-X (X= S, Se) bond lengths around the Sb2 site.

Figure 6 Variations of interatomic distances between the ribbons along the *b*-axis direction.

Figure 7 Variations of polyhedral volumes of $Sb1X_7$ and $Sb2X_7$ and their polyhedral eccentric parameters calculated by the IVTON program (Balić-Žunić and Vickovic 1996).

Figure 8 Molecular orbitals associated with the stereochemical activity of Sb $5s^2$ LPEs in (a) Sb_2S_3,

(b) $Sb_2(S_2Se)_3$, and (c) Sb_2Se_3. Sb atoms are shown as purple spheres, S atoms are yellow, and Se atoms are orange. The red and green colours orbitals represent positive and negative wavefunction, respectively. The orbitals are drawn at an isosurface value of 0.02. Contours of the electron density isosurface are plotted on the ac plane.

Table 1 Summarized crystal data and details of the refinement parameters for all crystals in the $Sb_2S_{3-x}Se_x$ solid solution

Table 2 Atomic coordinates, site occupancy parameters, equivalent isotropic, and anisotropic temperature factors ($Å^2$)

Table 3 Intra-ribbon and inter-ribbon distances (Å) in the $Sb_2S_{3-x}Se_x$ solid solution

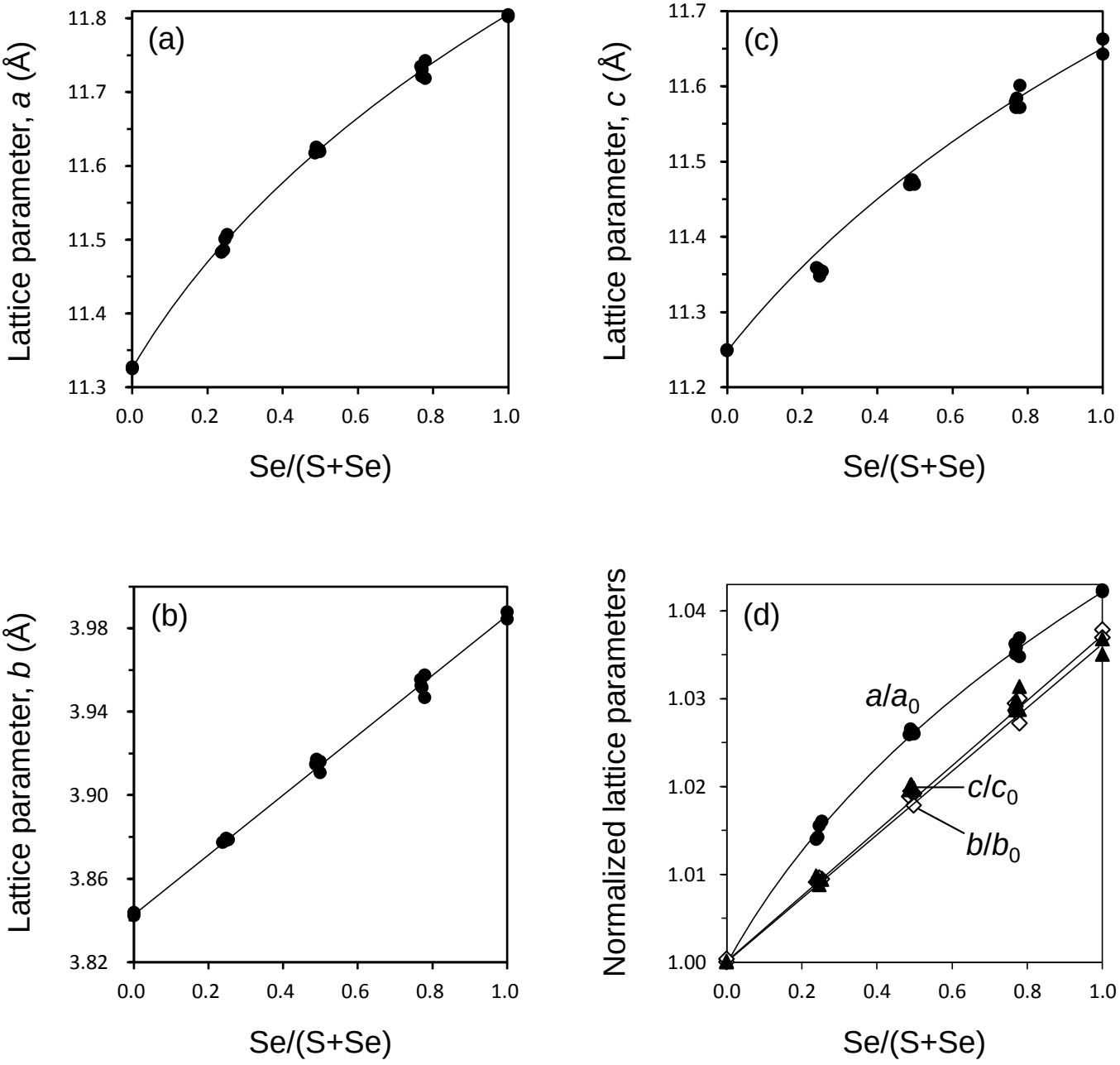

Figure 1. The compositional dependence lattice parameters of (a) *a*, (b) *b*, and (c) *c*. (d) The variations of normalized lattice parameters divided by minimum values for each lattice parameter. Solid circles, open diamonds, and solid triangles stand for the a/a_0, b/b_0, and c/c_0, respectively. Data were fitted by a least-squares regression to the second degree polynomial curve. The error bars are within the symbol size.

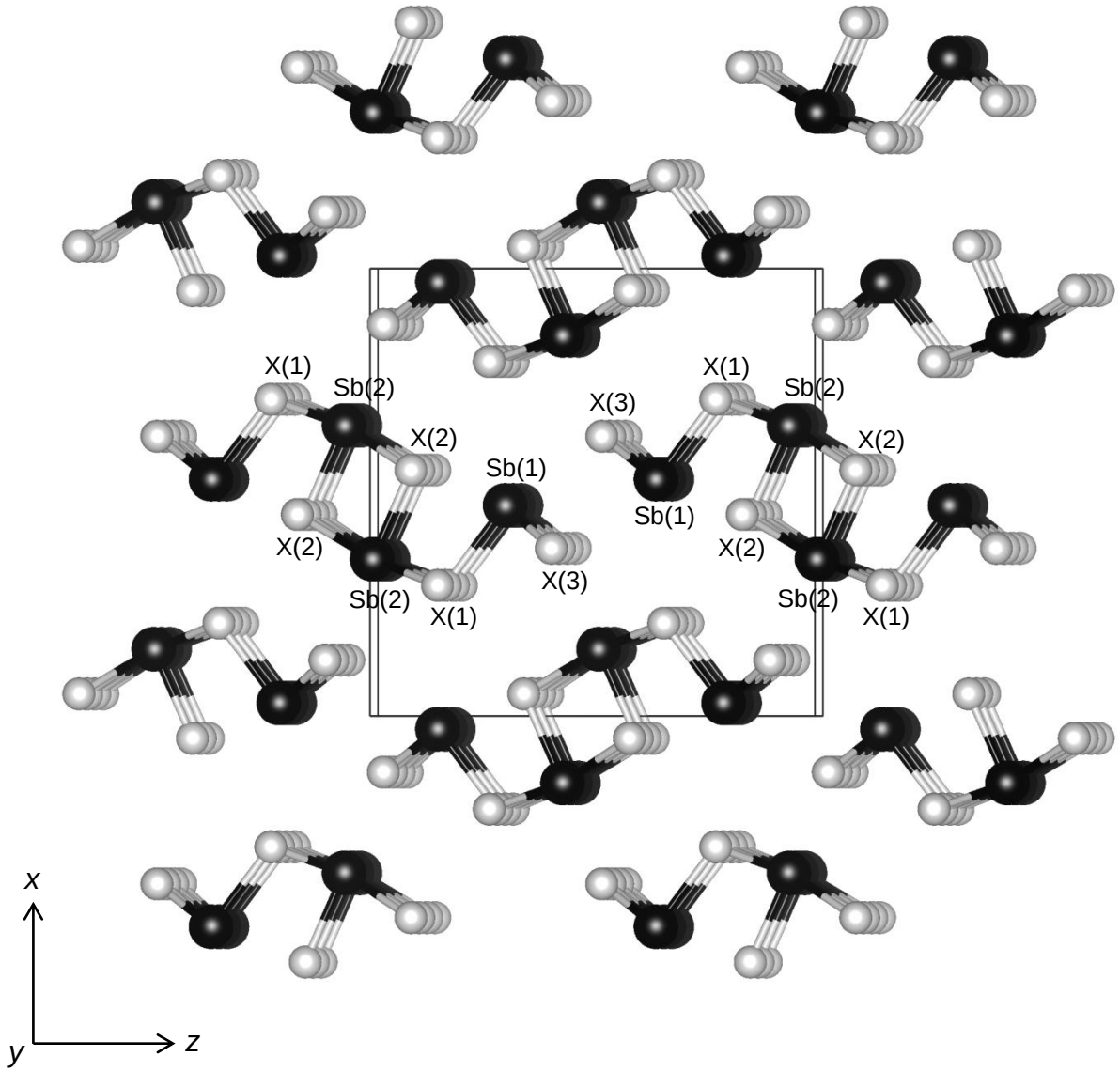

Figure 2. A ball-and-stick view of the crystal structure of Sb_2X_3 (X=S, Se) viewed in the direction of *b*-axis.

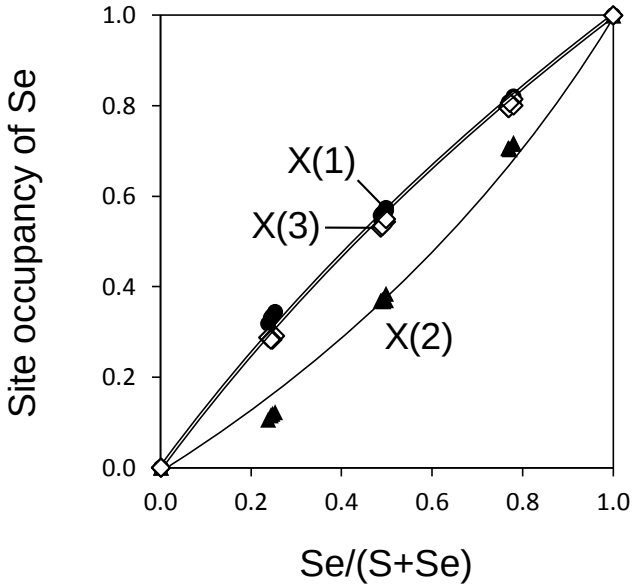

Figure 3. Site occupancy parameters of Se for the three X sites (X=S, Se) in the $Sb_2S_{3-x}Se_x$ solid solution. Solid circles, solid triangles, and open diamonds indicate the X(1), X(2), and X(3) site, respectively.

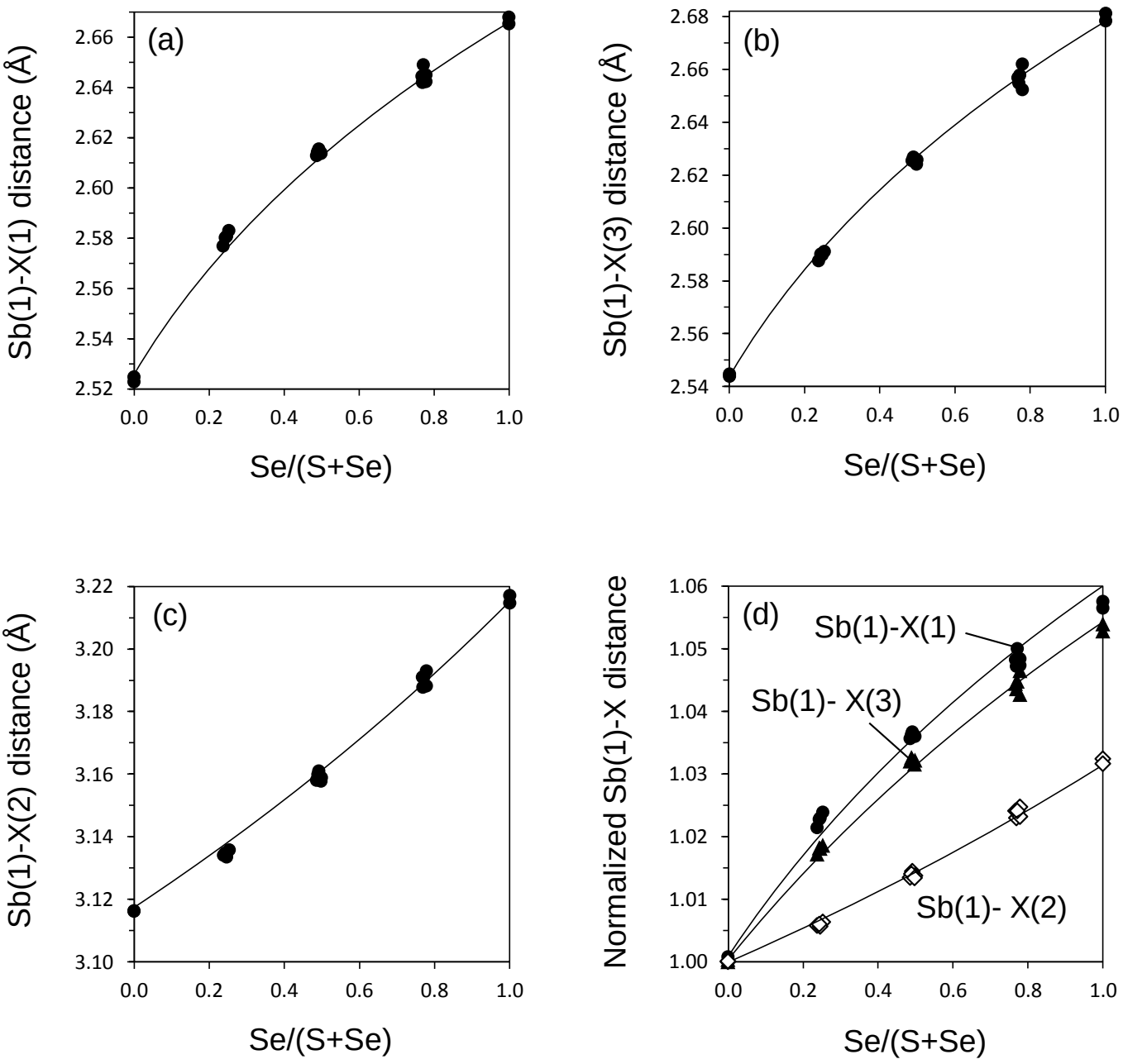

Figure 4. Variations of intra-ribbon Sb(1)-X (X= S, Se) distances. (d) The variations of normalized Sb(1)-X distance. Solid circles, open diamonds, and solid triangles stand for the Sb(1)-X(1), Sb(1)-X(2), and Sb(1)-X(3), respectively. The error bars are smaller than the symbol size.

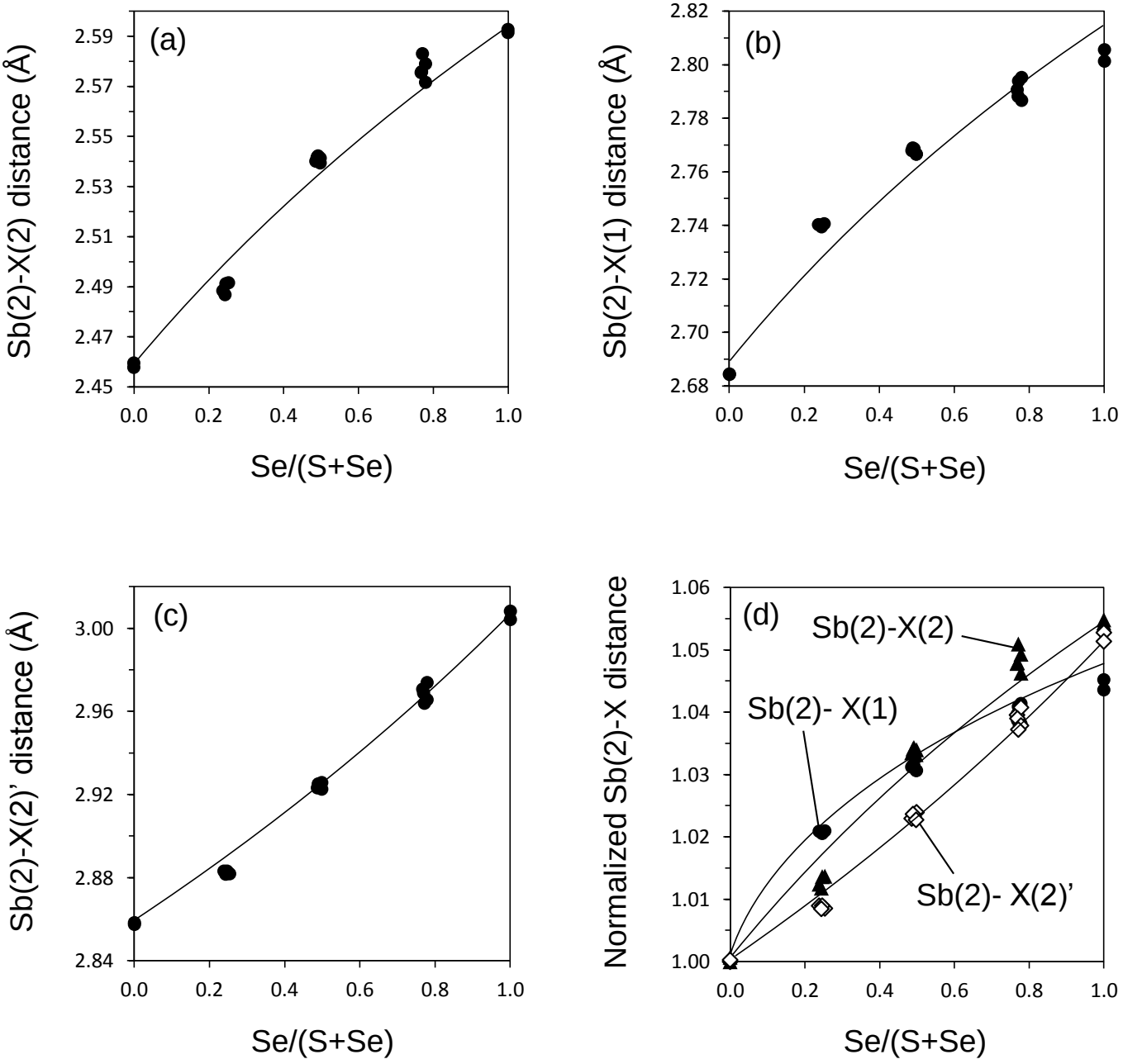

Figure 5. Variations of intra-ribbon Sb(2)-X (X= S, Se) distances. (d) The variations of normalized Sb(2)-X distance. Solid circles, open diamonds, and solid triangles display the Sb(2)-X(1), Sb(2)-X(2)', and Sb(2)-X(2), respectively.

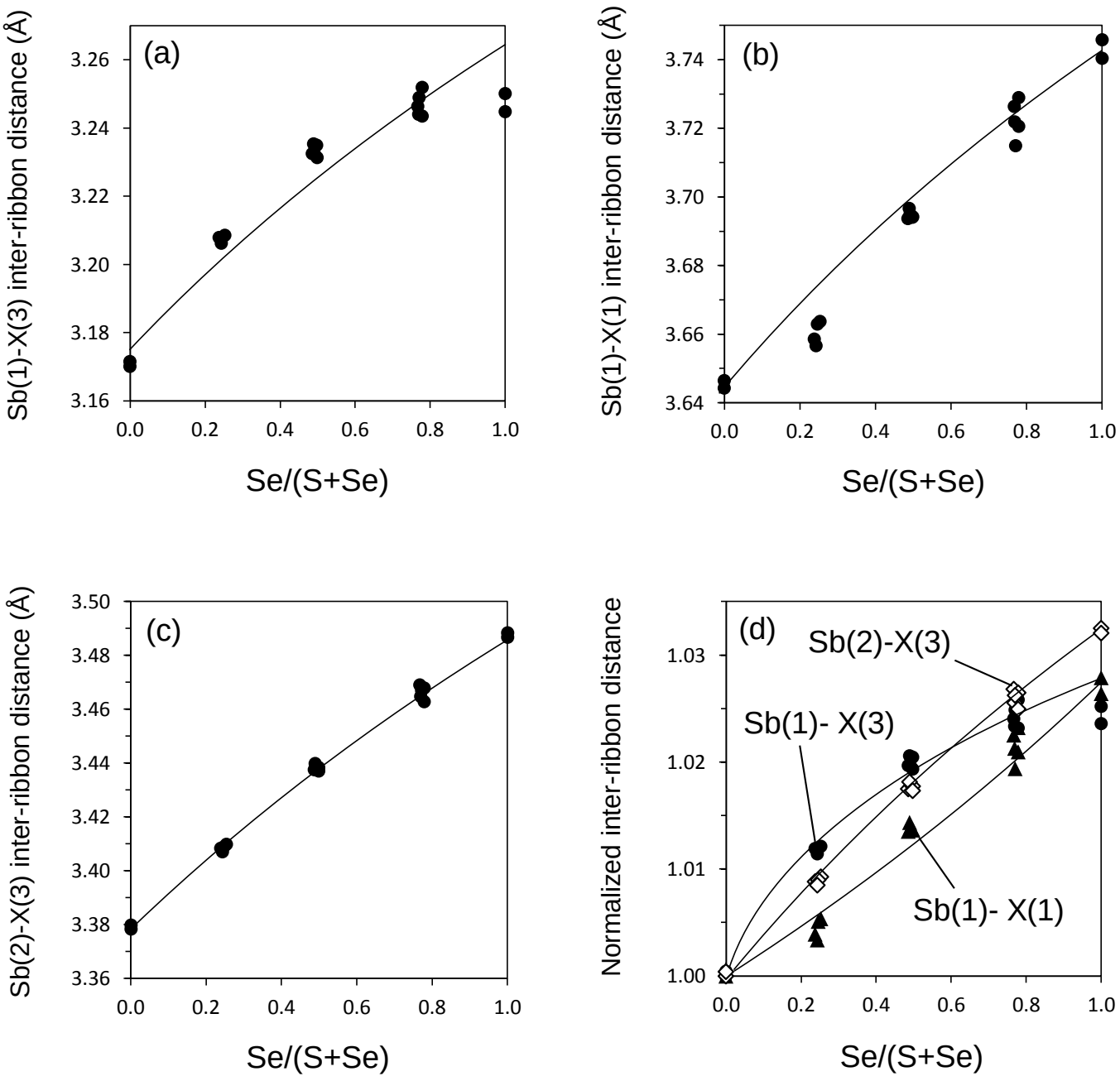

Figure 6. Variations of the inter-ribbon distances of Sb-X (X=S, Se). (d) The variations of normalized inter-ribbon distance. Solid circles, open diamonds, and solid triangles show the Sb(1)-X(3), Sb(2)-X(3), and Sb(1)-X(1), respectively.

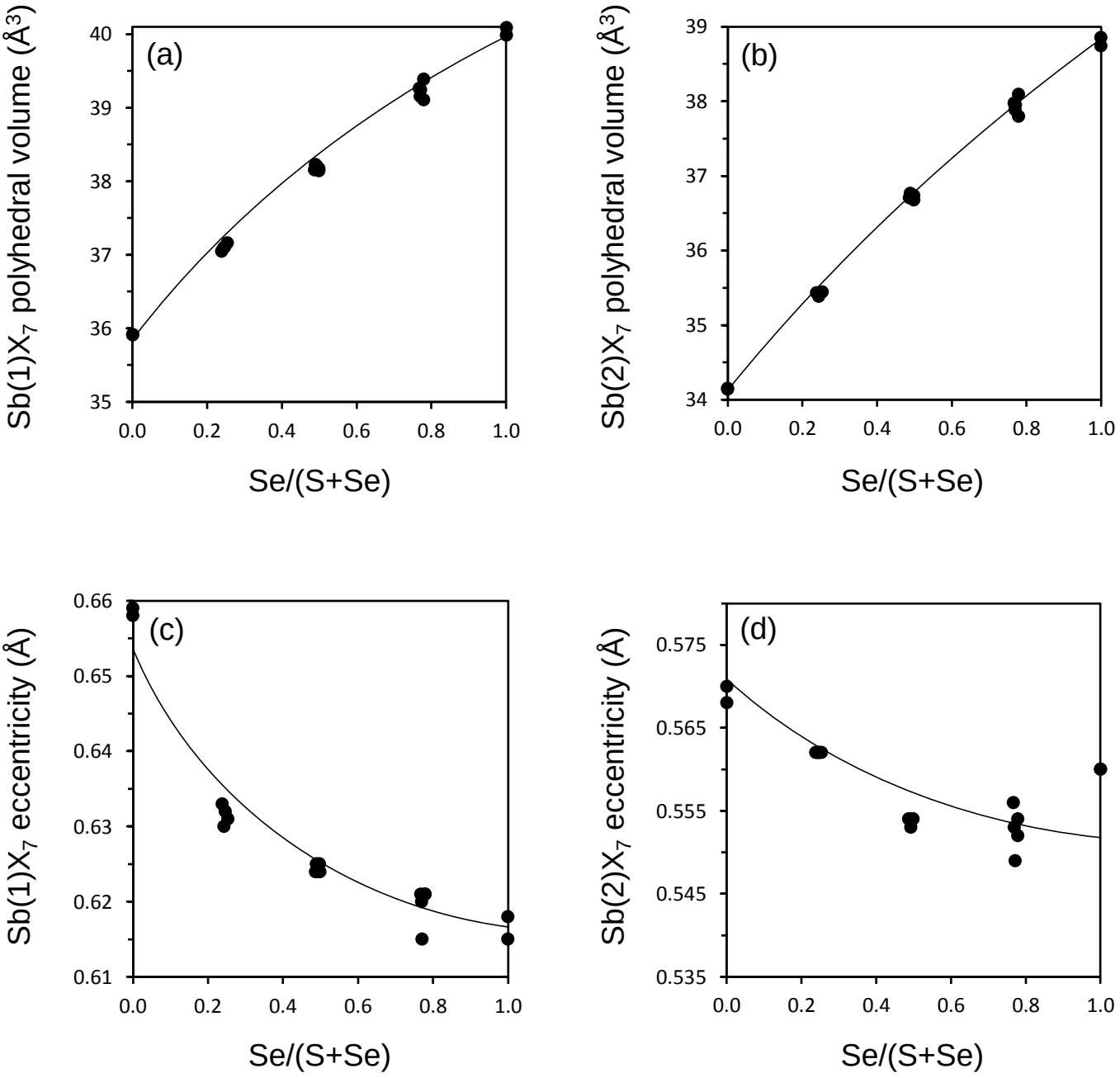

Figure 7. Variations of polyhedral volumes of $Sb(1)X_7$ and $Sb(2)X_7$ (X=S, Se) and their polyhedral eccentric parameters calculated by the IVTON program (Balić-Žunić and Vickovic 1996).

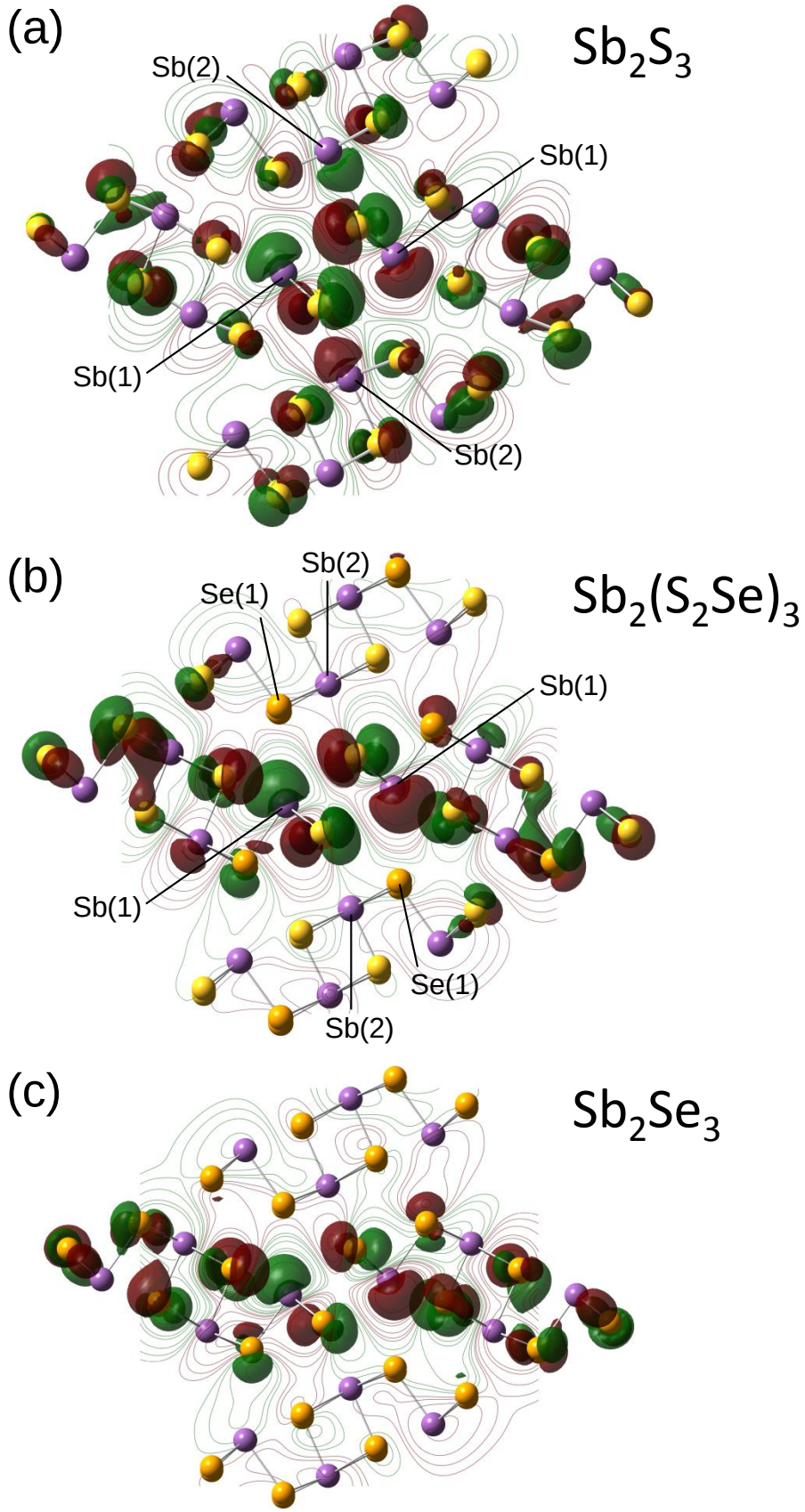

Figure 8. Molecular orbitals associated with the stereochemical activity of Sb $5s^2$ LPEs in (a) Sb_2S_3, (b) $Sb_2(S_2Se)_3$, and (c) Sb_2Se_3. Sb atoms are shown as purple spheres, S atoms are yellow, and Se atoms are orange. The red and green colours orbitals represent positive and negative wavefunction, respectively. The orbitals are drawn at an isosurface value of 0.02. Contours of the electron density isosurface are plotted on the *ac* plane.

Table 1. Summarized crystal data and details of the refinement parameters for all crystals in the $Sb_2S_{3-x}Se_x$ solid solution

Sample#	**S300Se0-1**	**S300Se0-2**	**S225Se075-1**	**S225Se075-5**	**S225Se075-6**
Chemical composition	Sb_2S_3	Sb_2S_3	$Sb_2S_{2.29}Se_{0.71}$	$Sb_2S_{2.24}Se_{0.76}$	$Sb_2S_{2.26}Se_{0.74}$
Crystal size (μm)	300 × 100 × 100	300 × 150 × 150	300 × 150 × 150	200 × 100 × 100	300 × 100 × 100
Crystal system	Orthorhombic	Orthorhombic	Orthorhombic	Orthorhombic	Orthorhombic
Space group	*Pnma*	*Pnma*	*Pnma*	*Pnma*	*Pnma*
Z	4	4	4	4	4
a (Å)	11.3276(17)	11.3252(18)	11.4834(11)	11.5070(10)	11.5011(9)
b (Å)	3.8423(6)	3.8437(4)	3.8773(3)	3.8787(3)	3.8792(2)
c (Å)	11.2484(18)	11.2498(17)	11.3589(8)	11.3543(9)	11.3475(9)
V (Å^3)	489.57(13)	489.71(12)	505.75(7)	506.77(7)	506.27(6)
D_{calc} (g/cm^3)	4.608	4.607	4.898	4.919	4.911
μ (cm^{-1})	121.055	121.021	165.363	168.419	167.227
Total reflections, R_{int}	4469, 0.059	4463, 0.056	4616, 0.087	4668, 0.073	4637, 0.058
Unique reflections	640	639	657	659	658
Observed ref. with $F_0 > 4s(F_o)$	570	568	592	620	621
Paraeters	32	32	44	44	44
*R*1	0.0314	0.0341	0.0511	0.0406	0.0349
*wR*2	0.0355	0.0413	0.0606	0.0472	0.0462
GooF	1.047	1.046	1.061	1.038	1.038

Sample#	**S225Se075-7**	**S150Se150-4**	**S150Se150-5**	**S150Se150-6**	**S150Se150-7**
Chemical composition	$Sb_2S_{2.27}Se_{0.73}$	$Sb_2S_{1.52}Se_{1.48}$	$Sb_2S_{1.54}Se_{1.46}$	$Sb_2S_{1.50}Se_{1.50}$	$Sb_2S_{1.53}Se_{1.47}$
Crystal size (μm)	300 × 100 × 100	200 × 50 × 50	200 × 100 × 100	200 × 100 × 100	200 × 50 × 50
Crystal system	Orthorhombic	Orthorhombic	Orthorhombic	Orthorhombic	Orthorhombic
Space group	*Pnma*	*Pnma*	*Pnma*	*Pnma*	*Pnma*
Z	4	4	4	4	4
a (Å)	11.4862(10)	11.6237(18)	11.6182(10)	11.6195(13)	11.626(3)
b (Å)	3.8779(3)	3.9153(4)	3.9148(2)	3.9161(3)	3.9171(7)
c (Å)	11.3567(7)	11.4756(15)	11.4687(8)	11.4696(10)	11.475(2)
V (Å^3)	505.85(7)	522.25(12)	521.62(6)	521.90(8)	522.59(19)
D_{calc} (g/cm^3)	4.909	5.203	5.197	5.218	5.193
μ (cm^{-1})	166.687	210.739	209.678	212.199	209.945
Total reflections, R_{int}	4666, 0.065	4764, 0.093	4796, 0.057	4759, 0.050	4350, 0.083
Unique reflections	657	678	679	679	673
Observed ref. with $F_0 > 4s(F_o)$	601	609	586	595	601
Parameters	44	44	44	44	44
*R*1	0.0389	0.0316	0.0297	0.0292	0.0505
*wR*2	0.0470	0.0309	0.0342	0.0404	0.0537
GooF	1.051	1.004	1.065	1.001	1.001

Table 1. Continued

Sample#	**S150Se150-8**	**S075Se225-1**	**S075Se225-2**	**S075Se225-3**	**S075Se225-9**
Chemical composition	$Sb_2S_{1.51}Se_{1.49}$	$Sb_2S_{0.70}Se_{2.30}$	$Sb_2S_{0.66}Se_{2.34}$	$Sb_2S_{0.69}Se_{2.31}$	$Sb_2S_{0.66Se2.34}$
Crystal size (μm)	300 × 100 × 100	100 × 50 × 50	200 × 100 × 100	200 × 50 × 50	200 × 50 × 50
Crystal system	Orthorhombic	Orthorhombic	Orthorhombic	Orthorhombic	Orthorhombic
Space group	*Pnma*	*Pnma*	*Pnma*	*Pnma*	*Pnma*
Z	4	4	4	4	4
a (Å)	11.622(2)	11.7354(17)	11.743(3)	11.7222(9)	11.7191(9)
b (Å)	3.9108(6)	3.9554(4)	3.9576(11)	3.9524(2)	3.9467(4)
c (Å)	11.4712(14)	11.5794(13)	11.601(4)	11.5714(6)	11.5716(8)
V (Å^3)	521.40(14)	537.50(11)	539.1(3)	536.12(6)	535.21(8)
D_{calc} (g/cm^3)	5.217	5.530	5.537	5.550	5.577
μ (cm^{-1})	211.744	257.121	258.901	258.424	260.785
Total reflections, R_{int}	4744, 0.079	4778, 0.074	4587, 0.118	4955, 0.078	4949, 0.083
Unique reflections	677	699	702	700	699
Observed ref. with $F_0 > 4s(F_o)$	618	578	544	575	597
Parameters	44	44	44	44	44
*R*1	0.0445	0.0353	0.0526	0.0314	0.0398
*wR*2	0.0529	0.0423	0.0647	0.0341	0.0462
GooF	1.062	1.025	1.002	1.022	1.048

Sample#	**S075Se225-10**	**S0Se300-1**	**S0Se300-3**
Chemical composition	$Sb_2S_{0.69}Se_{2.31}$	Sb_2Se_3	Sb_2Se_3
Crystal size (μm)	200 × 50 × 50	200 × 100 × 100	300 × 150 × 150
Crystal system	Orthorhombic	Orthorhombic	Orthorhombic
Space group	*Pnma*	*Pnma*	*Pnma*
Z	4	4	4
a (Å)	11.731(5)	11.805(2)	11.8026(7)
b (Å)	3.9516(13)	3.9877(6)	3.9843(3)
c (Å)	11.584(4)	11.6623(16)	11.6425(11)
V (Å^3)	537.0(3)	549.03(15)	547.49(7)
D_{calc} (g/cm^3)	5.541	5.811	5.828
μ (cm^{-1})	258.010	295.480	296.310
Total reflections, R_{int}	4817, 0.190	5069, 0.128	5062, 0.113
Unique reflections	701	714	711
Observed ref. with $F_0 > 4s(F_o)$	558	578	645
Parameters	44	32	32
*R*1	0.0554	0.0575	0.0566
*wR*2	0.0477	0.0676	0.0617
GooF	1.023	1.001	1.063

Table 2. Atomic coordinates, site occupancy parameters, equivalent isotropic, and anisotropic temperature factors ($Å^2$)

	x	*y*	*z*	B_{eq}	Site occupancy (S/Se)	U_{11}	U_{22}	U_{33}	U_{12}	U_{13}	U_{23}
S300Se0-1											
Sb_2S_3											
Sb(1)	0.47075(3)	0.25	0.32604(3)	1.151(6)		0.01506(16)	0.01162(16)	0.01704(18)	0	0.00156(13)	0
Sb(2)	0.35052(3)	0.75	0.03605(3)	1.472(6)		0.01396(16)	0.01793(18)	0.02405(19)	0	-0.00447(14)	0
X(1)	0.29216(10)	0.25	0.19204(11)	1.14(2)	1.000/0.000	0.0141(5)	0.0144(5)	0.0146(5)	0	-0.0004(4)	0
X(2)	0.54976(10)	0.75	0.12296(11)	1.11(2)	1.000/0.000	0.0127(4)	0.0129(5)	0.0166(5)	0	-0.0019(4)	0
X(3)	0.37500(10)	0.75	0.43881(11)	1.15(2)	1.000/0.000	0.0169(5)	0.0125(5)	0.0144(5)	0	0.0024(4)	0
S300Se0-2											
Sb_2S_3											
Sb(1)	0.47075(3)	0.25	0.32603(3)	1.523(7)		0.02117(19)	0.01914(19)	0.01756(19)	0	0.00167(12)	0
Sb(2)	0.35053(3)	0.75	0.03601(3)	1.827(7)		0.01954(19)	0.0255(2)	0.0244(2)	0	-0.00477(14)	0
X(1)	0.29205(11)	0.25	0.19184(10)	1.51(2)	1.000/0.000	0.0188(5)	0.0227(6)	0.0159(5)	0	-0.0012(4)	0
X(2)	0.54964(10)	0.75	0.12295(11)	1.48(2)	1.000/0.000	0.0201(5)	0.0196(6)	0.0165(6)	0	-0.0010(4)	0
X(3)	0.37508(11)	0.75	0.43861(11)	1.51(2)	1.000/0.000	0.0241(6)	0.0202(6)	0.0132(5)	0	0.0021(4)	0
S225Se075-1											
$Sb_2S_{2.29}Se_{0.71}$											
Sb(1)	0.47001(4)	0.25	0.32571(3)	1.630(10)		0.0231(2)	0.0157(2)	0.0231(2)	0	0.00205(16)	0
Sb(2)	0.35222(4)	0.75	0.03521(4)	1.886(11)		0.0222(2)	0.0207(3)	0.0288(2)	0	-0.00453(17)	0
X(1)	0.28808(10)	0.25	0.19290(8)	1.58(2)	0.682(2)/0.318(2)	0.0233(6)	0.0165(6)	0.0202(5)	0	-0.0034(4)	0
X(2)	0.55006(13)	0.75	0.12460(11)	1.55(3)	0.894(2)/0.106(2)	0.0223(8)	0.0151(8)	0.0214(7)	0	0.0017(5)	0
X(3)	0.37321(11)	0.75	0.44055(10)	1.71(2)	0.712(2)/0.288(2)	0.0266(7)	0.0183(7)	0.0200(6)	0	0.0027(4)	0
S225Se075-5											
$Sb_2S_{2.24}Se_{0.76}$											
Sb(1)	0.47008(2)	0.25	0.32573(2)	1.385(6)		0.01584(16)	0.01752(17)	0.01925(18)	0	0.00212(10)	0
Sb(2)	0.35225(2)	0.75	0.03511(3)	1.648(7)		0.01467(17)	0.02261(19)	0.02535(19)	0	-0.00493(11)	0
X(1)	0.28796(6)	0.25	0.19272(6)	1.425(15)	0.656(1)/0.344(1)	0.0183(3)	0.0196(4)	0.0163(3)	0	-0.0026(2)	0
X(2)	0.55004(7)	0.75	0.12441(9)	1.473(19)	0.877(1)/0.123(1)	0.0171(4)	0.0190(5)	0.0199(5)	0	0.0012(3)	0
X(3)	0.37296(6)	0.75	0.44070(7)	1.343(15)	0.708(1)/0.292(1)	0.0175(3)	0.0180(4)	0.0155(4)	0	0.0021(2)	0
S225Se075-6											
$Sb_2S_{2.26}Se_{0.74}$											
Sb(1)	0.47001(2)	0.25	0.32572(2)	1.419(5)		0.01758(14)	0.01546(15)	0.02087(16)	0	0.00198(8)	0
Sb(2)	0.35219(2)	0.75	0.03515(2)	1.687(6)		0.01655(14)	0.02052(16)	0.02701(16)	0	-0.00509(8)	0
X(1)	0.28798(5)	0.25	0.19273(5)	1.444(11)	0.664(1)/0.336(1)	0.0190(2)	0.0178(3)	0.0181(2)	0	-0.0030(2)	0
X(2)	0.55002(6)	0.75	0.12457(7)	1.465(14)	0.881(1)/0.119(1)	0.0180(3)	0.0162(4)	0.0215(3)	0	0.0009(2)	0
X(3)	0.37298(5)	0.75	0.44062(5)	1.396(11)	0.716(1)/0.284(1)	0.0194(2)	0.0162(3)	0.0175(3)	0	0.0021(2)	0

Table 2. Continued

	x	*y*	*z*	B_{eq}	Site occupancy (S/Se)	U_{11}	U_{22}	U_{33}	U_{12}	U_{13}	U_{23}
S225Se075-7											
$Sb_2S_{2.27}Se_{0.73}$											
Sb(1)	0.47009(3)	0.25	0.32568(3)	1.489(7)		0.02071(19)	0.01294(17)	0.02291(19)	0	0.00194(12)	0
Sb(2)	0.35224(3)	0.75	0.03516(3)	1.753(7)		0.01990(19)	0.01779(19)	0.02890(19)	0	-0.00488(13)	0
X(1)	0.28793(7)	0.25	0.19272(6)	1.483(17)	0.669(1)/0.331(1)	0.0226(4)	0.0142(4)	0.0196(4)	0	-0.0029(2)	0
X(2)	0.54996(9)	0.75	0.12440(9)	1.51(2)	0.884(2)/0.116(1)	0.0214(5)	0.0129(5)	0.0232(5)	0	0.0015(3)	0
X(3)	0.37309(8)	0.75	0.44076(7)	1.478(18)	0.717(1)/0.283(1)	0.0224(4)	0.0139(4)	0.0199(4)	0	0.0020(2)	0
S150Se150-4											
$Sb_2S_{1.52}Se_{1.48}$											
Sb(1)	0.46970(5)	0.25	0.32629(6)	1.588(11)		0.0207(2)	0.0178(2)	0.0218(3)	0	0.0020(2)	0
Sb(2)	0.35290(5)	0.75	0.03625(5)	1.857(12)		0.0200(2)	0.0225(3)	0.0281(3)	0	-0.0055(2)	0
X(1)	0.28700(9)	0.25	0.19325(10)	1.43(2)	0.436(2)/0.564(2)	0.0201(6)	0.0171(6)	0.0171(6)	0	-0.0013(4)	0
X(2)	0.55245(11)	0.75	0.12691(11)	1.51(2)	0.632(2)/0.368(2)	0.0206(7)	0.0158(6)	0.0208(8)	0	0.0017(5)	0
X(3)	0.37184(9)	0.75	0.44224(10)	1.44(2)	0.456(2)/0.544(2)	0.0213(6)	0.0172(5)	0.0160(6)	0	0.0016(4)	0
S150Se150-5											
$Sb_2S_{1.54}Se_{1.46}$											
Sb(1)	0.46960(3)	0.25	0.32614(3)	1.534(6)		0.01950(18)	0.01653(17)	0.02227(17)	0	0.00213(13)	0
Sb(2)	0.35294(3)	0.75	0.03622(3)	1.807(7)		0.01863(19)	0.0214(2)	0.02861(19)	0	-0.00564(14)	0
X(1)	0.28695(6)	0.25	0.19323(6)	1.384(14)	0.443(1)/0.557(1)	0.0186(3)	0.0170(3)	0.0170(3)	0	-0.0019(2)	0
X(2)	0.55237(7)	0.75	0.12698(7)	1.484(17)	0.631(1)/0.369(1)	0.0207(4)	0.0150(4)	0.0207(4)	0	0.0018(2)	0
X(3)	0.37188(6)	0.75	0.44223(6)	1.322(15)	0.467(1)/0.533(1)	0.0185(3)	0.0148(3)	0.0169(3)	0	0.0020(2)	0
S150Se150-6											
$Sb_2S_{1.50}Se_{1.50}$											
Sb(1)	0.46963(4)	0.25	0.32624(4)	1.622(8)		0.0222(2)	0.01807(19)	0.0214(2)	0	0.00187(16)	0
Sb(2)	0.35290(4)	0.75	0.03645(4)	1.909(8)		0.0214(2)	0.0227(2)	0.0285(2)	0	-0.00547(18)	0
X(1)	0.28698(7)	0.25	0.19323(7)	1.525(17)	0.432(2)/0.568(2)	0.0225(4)	0.0188(4)	0.0167(4)	0	-0.0019(3)	0
X(2)	0.55248(8)	0.75	0.12708(8)	1.61(2)	0.616(2)/0.384(2)	0.0237(5)	0.0171(4)	0.0205(5)	0	0.0028(3)	0
X(3)	0.37187(7)	0.75	0.44226(7)	1.465(17)	0.456(2)/0.544(2)	0.0220(4)	0.0176(4)	0.0160(4)	0	0.0019(3)	0
S150Se150-7											
$Sb_2S_{1.53}Se_{1.47}$											
Sb(1)	0.46959(3)	0.25	0.32612(4)	1.484(9)		0.0191(2)	0.0170(2)	0.0203(2)	0	0.00195(15)	0
Sb(2)	0.35293(4)	0.75	0.03625(5)	1.761(9)		0.0188(2)	0.0216(2)	0.0265(2)	0	-0.00546(17)	0
X(1)	0.28698(7)	0.25	0.19318(8)	1.390(18)	0.438(2)/0.562(2)	0.0185(4)	0.0186(4)	0.0157(4)	0	-0.0021(2)	0
X(2)	0.55237(8)	0.75	0.12697(9)	1.45(2)	0.628(2)/0.372(2)	0.0190(5)	0.0163(5)	0.0199(6)	0	0.0015(3)	0
X(3)	0.37185(7)	0.75	0.44217(9)	1.311(18)	0.466(2)/0.534(2)	0.0191(4)	0.0164(4)	0.0143(5)	0	0.0021(2)	0

Table 2. Continued

	x	*y*	*z*	B_{eq}	Site occupancy (S/Se)	U_{11}	U_{22}	U_{33}	U_{12}	U_{13}	U_{23}
S150Se150-8											
$Sb_2S_{1.51}Se_{1.49}$											
Sb(1)	0.46956(4)	0.25	0.32611(4)	1.357(9)		0.0188(2)	0.0140(2)	0.0187(2)	0	0.00188(15)	0
Sb(2)	0.35293(4)	0.75	0.03633(4)	1.629(10)		0.0186(2)	0.0185(2)	0.0248(2)	0	-0.00526(17)	0
X(1)	0.28683(7)	0.25	0.19325(7)	1.254(18)	0.426(2)/0.574(2)	0.0184(4)	0.0141(4)	0.0152(4)	0	-0.0027(2)	0
X(2)	0.55231(9)	0.75	0.12688(8)	1.30(2)	0.630(2)/0.370(2)	0.0198(6)	0.0116(5)	0.0178(6)	0	0.0014(3)	0
X(3)	0.37180(7)	0.75	0.44217(8)	1.164(19)	0.450(2)/0.550(2)	0.0182(5)	0.0129(4)	0.0132(4)	0	0.0014(2)	0
S075Se225-1											
$Sb_2S_{0.70}Se_{2.30}$											
Sb(1)	0.46948(4)	0.25	0.32711(4)	1.570(9)		0.0231(2)	0.0164(2)	0.0201(2)	0	0.00228(19)	0
Sb(2)	0.35299(4)	0.75	0.03802(5)	1.821(10)		0.0215(2)	0.0215(2)	0.0262(2)	0	-0.00481(19)	0
X(1)	0.28633(7)	0.25	0.19405(7)	1.447(17)	0.202(2)/0.798(2)	0.0215(4)	0.0179(4)	0.0155(4)	0	-0.0015(3)	0
X(2)	0.55355(7)	0.75	0.12834(7)	1.549(18)	0.294(2)/0.706(2)	0.0231(5)	0.0163(4)	0.0194(4)	0	0.0008(3)	0
X(3)	0.37129(6)	0.75	0.44363(7)	1.479(17)	0.204(2)/0.796(2)	0.0234(5)	0.0170(4)	0.0158(4)	0	0.0021(2)	0
S075Se225-2											
$Sb_2S_{0.66}Se_{2.34}$											
Sb(1)	0.46953(9)	0.25	0.32699(10)	1.82(2)		0.0239(5)	0.0209(5)	0.0243(5)	0	0.0025(4)	0
Sb(2)	0.35287(9)	0.75	0.03792(10)	2.08(2)		0.0236(6)	0.0251(5)	0.0303(6)	0	-0.0054(4)	0
X(1)	0.28639(15)	0.25	0.19425(14)	1.66(4)	0.194(4)/0.806(4)	0.0222(11)	0.0220(10)	0.0188(9)	0	-0.0010(6)	0
X(2)	0.55354(15)	0.75	0.12837(15)	1.76(4)	0.284(4)/0.716(4)	0.0241(12)	0.0202(9)	0.0224(10)	0	0.0015(7)	0
X(3)	0.37111(14)	0.75	0.44379(15)	1.80(4)	0.186(4)/0.814(4)	0.0258(12)	0.0226(8)	0.0200(10)	0	0.0030(6)	0
S075Se225-3											
$Sb_2S_{0.69}Se_{2.31}$											
Sb(1)	0.46949(4)	0.25	0.32704(4)	1.392(8)		0.0165(2)	0.0161(2)	0.0203(2)	0	0.00235(18)	0
Sb(2)	0.35283(4)	0.75	0.03796(4)	1.664(9)		0.0155(2)	0.0212(2)	0.0266(2)	0	-0.00468(19)	0
X(1)	0.28632(6)	0.25	0.19400(6)	1.313(16)	0.192(2)/0.808(2)	0.0156(3)	0.0180(4)	0.0162(4)	0	-0.0015(2)	0
X(2)	0.55361(6)	0.75	0.12840(7)	1.369(17)	0.294(2)/0.706(2)	0.0169(4)	0.0157(4)	0.0194(4)	0	0.0008(3)	0
X(3)	0.37135(6)	0.75	0.44361(7)	1.283(16)	0.206(2)/0.794(2)	0.0167(4)	0.0161(3)	0.0159(4)	0	0.0017(2)	0
S075Se225-9											
$Sb_2S_{0.66}Se_{2.34}$											
Sb(1)	0.46947(4)	0.25	0.32717(4)	1.338(10)		0.0174(2)	0.0135(2)	0.0200(2)	0	0.0022(2)	0
Sb(2)	0.35297(4)	0.75	0.03802(5)	1.584(10)		0.0164(2)	0.0183(2)	0.0255(2)	0	-0.0047(2)	0
X(1)	0.28627(7)	0.25	0.19406(7)	1.301(18)	0.180(2)/0.820(2)	0.0167(4)	0.0164(5)	0.0163(4)	0	-0.0012(3)	0
X(2)	0.55352(7)	0.75	0.12822(7)	1.321(19)	0.282(2)/0.712(2)	0.0172(5)	0.0140(4)	0.0190(4)	0	0.0007(3)	0
X(3)	0.37121(7)	0.75	0.44362(8)	1.241(18)	0.200(2)/0.800(2)	0.0170(4)	0.0145(4)	0.0157(4)	0	0.0021(3)	0

Table 2. Continued

	x	*y*	*z*	B_{eq}	Site occupancy (S/Se)	U_{11}	U_{22}	U_{33}	U_{12}	U_{13}	U_{23}
S075Se225-10											
$Sb_2S_{0.69}Se_{2.31}$											
Sb(1)	0.4696(2)	0.25	0.32673(15)	2.28(4)		0.0384(15)	0.0224(9)	0.0260(9)	0	0.0037(10)	0
Sb(2)	0.3529(2)	0.75	0.03776(15)	2.36(4)		0.0326(15)	0.0266(10)	0.0305(11)	0	-0.0054(10)	0
X(1)	0.2856(3)	0.25	0.1941(2)	2.34(9)	0.196(8)/0.804(8)	0.039(2)	0.028(2)	0.0227(18)	0	-0.0017(15)	0
X(2)	0.5542(3)	0.75	0.1281(2)	2.33(9)	0.296(7)/0.704(7)	0.038(3)	0.0234(19)	0.027(2)	0	-0.0023(17)	0
X(3)	0.3714(3)	0.75	0.4436(2)	2.21(8)	0.194(7)/0.806(7)	0.036(2)	0.0213(18)	0.0263(19)	0	0.0022(19)	0
S0Se300-1											
Sb_2Se_3											
Sb(1)	0.46976(9)	0.25	0.32795(8)	1.72(2)		0.0264(6)	0.0150(5)	0.0238(5)	0	0.0020(4)	0
Sb(2)	0.35265(10)	0.75	0.03946(9)	1.89(2)		0.0243(6)	0.0183(5)	0.0291(6)	0	-0.0027(4)	0
X(1)	0.28627(13)	0.25	0.19480(12)	1.58(3)	0.000/1.000	0.0237(9)	0.0161(8)	0.0203(8)	0	-0.0010(6)	0
X(2)	0.55363(14)	0.75	0.12881(12)	1.58(3)	0.000/1.000	0.0248(9)	0.0136(7)	0.0218(8)	0	0.0004(6)	0
X(3)	0.37100(13)	0.75	0.44472(13)	1.56(3)	0.000/1.000	0.0267(9)	0.0146(7)	0.0177(8)	0	0.0015(6)	0
S0Se300-3											
Sb_2Se_3											
Sb(1)	0.46987(4)	0.25	0.32798(6)	1.415(13)		0.0200(3)	0.0107(3)	0.0231(4)	0	0.00187(19)	0
Sb(2)	0.35256(4)	0.75	0.03955(6)	1.657(14)		0.0179(3)	0.0154(3)	0.0297(4)	0	-0.0037(2)	0
X(1)	0.28600(6)	0.25	0.19467(8)	1.239(18)	0.000/1.000	0.0171(4)	0.0120(4)	0.0180(5)	0	-0.0006(2)	0
X(2)	0.55386(6)	0.75	0.12871(8)	1.255(17)	0.000/1.000	0.0174(3)	0.0110(4)	0.0193(5)	0	-0.0005(2)	0
X(3)	0.37109(6)	0.75	0.44467(9)	1.273(18)	0.000/1.000	0.0183(4)	0.0113(4)	0.0187(5)	0	0.0021(2)	0

Table 3. Intra-ribbon and inter-ribbon distances (Å) in the $Sb_2S_{3-x}Se_x$ solid solution

Sample#	Chemical composition	Intra-ribbon distances (Å)						Inter-ribbon distances (Å)		
		Sb(1)- X(1)	Sb(1)- X(3) X(3)[1]	Sb(1)- X(2) X(2)[1]	Sb(2)- X(1) X(1)[2]	Sb(2)- X(2)	Sb(2)- X(2)[3] X(2)[4]	Sb(1)- X(3)[5]	Sb(1)- X(1)[6]	Sb2- X(3)[7] X(3)[8]
S300Se0-1	Sb_2S_3	2.523 (1)	2.5448 (8)	3.1161 (9)	2.6845 (8)	2.460 (1)	2.8576 (9)	3.170 (1)	3.647 (1)	3.3783 (9)
S300Se0-2	Sb_2S_3	2.525 (1)	2.5439 (8)	3.1163 (9)	2.6843 (8)	2.458 (1)	2.8583 (9)	3.172 (1)	3.644 (1)	3.380 (1)
S225Se075-1	$Sb_2S_{2.29}Se_{0.71}$	2.577 (1)	2.5876 (8)	3.134 (1)	2.7403 (7)	2.488 (1)	2.883 (1)	3.208 (1)	3.659 (1)	3.408 (1)
S225Se075-5	$Sb_2S_{2.24}Se_{0.76}$	2.5831 (7)	2.5912 (5)	3.1357 (8)	2.7406 (5)	2.4916 (8)	2.8820 (7)	3.2086 (7)	3.6638 (7)	3.4097 (6)
S225Se075-6	$Sb_2S_{2.26}Se_{0.74}$	2.5808 (6)	2.5899 (4)	3.1335 (6)	2.7395 (4)	2.4913 (7)	2.8831 (5)	3.2080 (6)	3.6630 (6)	3.4087 (5)
S225Se075-7	$Sb_2S_{2.27}Se_{0.73}$	2.5803 (8)	2.5902 (6)	3.1347 (8)	2.7399 (5)	2.487 (1)	2.8818 (8)	3.2063 (9)	3.6567 (8)	3.4070 (7)
S150Se150-4	$Sb_2S_{1.52}Se_{1.48}$	2.616 (1)	2.6262 (8)	3.161 (1)	2.7686 (8)	2.542 (1)	2.924 (1)	3.232 (1)	3.695 (1)	3.4381 (9)
S150Se150-5	$Sb_2S_{1.54}Se_{1.46}$	2.6128 (7)	2.6255 (5)	3.1580 (6)	2.7680 (5)	2.5401 (8)	2.9232 (6)	3.2325 (7)	3.6937 (7)	3.4374 (6)
S150Se150-6	$Sb_2S_{1.50}Se_{1.50}$	2.6137 (9)	2.6259 (6)	3.1589 (8)	2.7666 (6)	2.541 (1)	2.9259 (7)	3.2314 (9)	3.6942 (9)	3.4383 (7)
S150Se150-7	$Sb_2S_{1.53}Se_{1.47}$	2.6143 (9)	2.6269 (6)	3.1598 (8)	2.7689 (7)	2.542 (1)	2.9251 (8)	3.235 (1)	3.6967 (8)	3.4397 (8)
S150Se150-8	$Sb_2S_{1.51}Se_{1.49}$	2.6140 (9)	2.6243 (6)	3.1578 (8)	2.7666 (6)	2.539 (1)	2.9226 (7)	3.2350 (9)	3.6941 (9)	3.4369 (7)
S075Se225-1	$Sb_2S_{0.70}Se_{2.30}$	2.6445 (9)	2.6570 (6)	3.1910 (7)	2.7906 (6)	2.5755 (9)	2.9707 (7)	3.2464 (9)	3.7264 (9)	3.4689 (7)
S075Se225-2	$Sb_2S_{0.66}Se_{2.34}$	2.645 (2)	2.662 (1)	3.193 (1)	2.795 (1)	2.579 (2)	2.974 (1)	3.252 (2)	3.729 (2)	3.468 (1)
S075Se225-3	$Sb_2S_{0.69}Se_{2.31}$	2.6420 (8)	2.6549 (5)	3.1877 (7)	2.7881 (5)	2.5758 (8)	2.9689 (6)	3.2441 (9)	3.7219 (8)	3.4646 (7)
S075Se225-9	$Sb_2S_{0.66Se2.34}$	2.6423 (9)	2.6525 (6)	3.1882 (7)	2.7867 (6)	2.5716 (9)	2.9658 (7)	3.244 (1)	3.7207 (9)	3.4626 (7)
S075Se225-10	$Sb_2S_{0.69}Se_{2.31}$	2.649 (4)	2.658 (2)	3.191 (2)	2.794 (2)	2.583 (4)	2.964 (2)	3.249 (3)	3.715 (4)	3.467 (3)
S0Se300-1	Sb_2Se_3	2.665 (1)	2.681 (1)	3.217 (1)	2.806 (1)	2.591 (1)	3.008 (1)	3.250 (1)	3.746 (1)	3.488 (1)
S0Se300-3	Sb_2Se_3	2.6680 (9)	2.6784 (7)	3.2146 (8)	2.8013 (7)	2.5927 (9)	3.0043 (8)	3.245 (1)	3.7405 (8)	3.487 (1)

Symmetry operations: 1, x , y -1, z ; 2, x , y +1, z ; 3, -x +1, -y +1, -z ; 4, -x +1, -y +2, -z ; 5, -x +1, -y +1, -z +1; 6, x +1/2, -y +1/2, -z +1/2; 7, -x +1/2, y +1/2, z -1/2; 8, -x +1/2, y -1/2, z -1/2.